Advanced Course and Workshop on Blood Flow
BF 2005 – (pp.205–242) – Warsaw, 2005.

Heat Transfer in Humans—Local and Whole-Body

G.M.J. Van Leeuwen and A.A. Van Steenhoven

Technische Universiteit Eindhoven
Postbus 513, 5600 MB, Eindhoven, the Netherlands
g.m.j.v.leeuwen@tue.nl

Temperature plays an important role in the functioning of biological (sub)systems. Here, efforts that have been made to calculate temperature distributions in humans will be reviewed. First, attention will be on the small scale. Different ways of modelling the crucial influence of blood flow will be described. The collective effect is reasonably successfully described by a heatsink. Predicting detailed inhomogeneous temperature distributions requires accounting for effects of individual vessels. Second, aspects involved in calculating an overall temperature distribution in different environmental conditions will be explained. Main mechanisms with which the body maintains its core temperature are vasoaction, sweating and shivering.

Key words: *Tissue heat transfer, bio heat equation, discrete vessel thermal model, thermoregulation.*

1. Introduction

Temperature influences the functioning of biological (sub)systems. Mammals are homeothermic: normally core temperature varies only within narrow bounds. For humans, normal core temperature is about 37°C. Even small differences in this temperature may have significant consequences for the behaviour of individual cells and the body as a whole. These temperature dependencies of biological processes can be used to clinical effect. There are several situations in which clinicians want to change the temperature of the whole body or part of the body. One example is the induction of higher temperatures (43°C) in a tumour as an adjuvant therapy against cancer (hyperthermia therapy); another example is the cooling of patients during surgery to protect sensitive tissues. Taking action might also be necessary to

maintain/restore normal temperature, e.g. when environmental conditions are harsh, to prevent morbidity or performance degradation. Examples are hypothermic low birth-weight babies, and athletes competing in high temperatures. It also works the other way: the functioning of biological systems influences their temperature. Hence, measurement of temperature can be used in clinical diagnosis (e.g. Fig. 1). Core temperature is routinely measured to monitor progress of disease and recovery; local temperature elevations can indicate infections or tumours.

Figure 1. A common clinical diagnostic device: the simple oral or rectal thermometer.

In order to control the temperature or just to monitor it, an understanding is necessary of the heat transfer processes within the human body and between the human body and the environment. This understanding is necessary to predict the outcome of thermal interventions (e.g. predict power density of heating system necessary for a desired rise in tumour temperature in local hyperthermia), and/or to provide information on temperature where it would otherwise be limited due to limitations on (invasive) thermometry.

This text will look at the processes taking place and at different types of models that have been developed to describe these. It will both look at the physics of heat transfer (the passive system), and at the thermoregulatory processes that take place to maintain a steady core temperature. It will become clear that the convective heat transfer by the blood plays a very important role in the development of temperatures both on the scale of the whole-body and on a local scale.

2. Heat Transfer within the Tissue; Continuum Models

2.1. Tissue Equations; Heat Sink and Effective Conductivity

Heat transfer within the body takes place by means of conduction and convection. Conduction is the transfer of heat from hot to cold via transfer of kinetic energy of constituting particles, without net displacement of the particles themselves. In an isotropic medium the conductive heat flow density $\phi_{\mathbf{k}}$

$[\mathrm{Wm}^{-2}]$ is governed by Fourier's law: $\phi_{\mathbf{k}} = -k\nabla T$ with k $[\mathrm{Wm}^{-1}\mathrm{K}^{-1}]$ the thermal conductivity of the medium. Generation of heat in a tissue volume element must lead to net outflow of heat from the element, or to heating of the tissue:

$$M = -\nabla \cdot k_{\mathrm{tis}} \nabla T + \rho_{\mathrm{tis}} c_{\mathrm{tis}} \frac{\partial T}{\partial t}$$

with M the volumetric rate of heat generation (metabolic rate and possibly absorbed power) $[\mathrm{Wm}^{-3}]$, ρ_{tis} the tissue density $[\mathrm{kg\,m}^{-3}]$, and c_{tis} the tissue specific heat $[\mathrm{Jkg}^{-1}\mathrm{K}^{-1}]$. Should the conductivity be uniform, and the problem stationary, this equation reduces to the Laplace equation, which for some simple cases can be analytically solved. Within the human body, pure conduction problems are very rare because most of the body is perfused by blood.

Heat may also be transferred due to flow of a medium: convection. Convective heat transfer is governed by a set of equations describing conservation of mass, momentum, and energy. Here, simultaneously solving them for the detailed blood vessel network will not be attempted. The importance of the convective heat transfer by the blood for body temperatures may be deduced from the fact that the human heart typically pumps 5 liter blood per minute through the body. If this is multiplied by the density and by the specific heat it is seen that the cardiac output is equivalent to about $300\,\mathrm{WK}^{-1}$. This means that if the blood changes on average just 0.25 K in temperature on its journey through the body it redistributes almost the same amount of heat as is produced by an average human in rest.

There are roughly 100 thousand kilometer of blood vessels within the body along which the blood-tissue heat transfer takes place. So, in an average $(10\,\mathrm{cm})^3$ cube of tissue there is more than a thousand kilometers of blood vessels present. That is a lot of surface area for the blood to exchange heat with the tissue. It should be obvious that it will be difficult to compute a detailed temperature distribution in even a very small part of the body accounting for all the blood vessels individually. Fortunately, the thermal effect of the blood vessels can be described collectively with some success.

In 1948 Harry H. Pennes [1] devised what has become known as the bio heat equation, or alternatively the heatsink equation, in which the effect of all vessels is lumped together.

$$\rho_{\mathrm{tis}} c_{\mathrm{tis}} \frac{\partial T}{\partial t} = \nabla \cdot k_{\mathrm{tis}} \nabla T - c_{\mathrm{b}} W_{\mathrm{b}} (T - T_{\mathrm{art}}) + M. \tag{2.1}$$

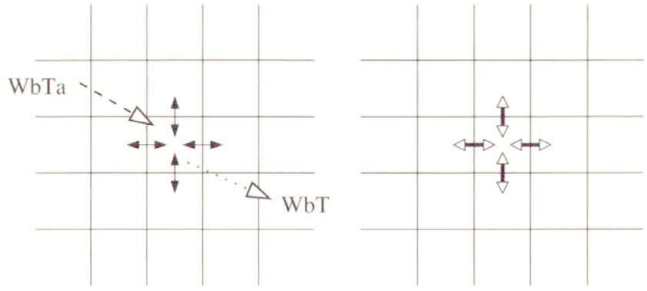

Figure 2. Two dimensional representation of the heat transferred into and out of a tissue element for the Pennes heatsink model and the limited k_{eff} model.

This continuum equation has one extra term with respect to the conduction equation. In this term, c_{b} is the specific heat of blood, W_{b} the blood perfusion in the tissue $\left[\text{kg}\,\text{m}^{-3}\,\text{s}^{-1}\right]$, and T_{art} the temperature of the arterial blood entering the volume. The bio heat equation describes blood to tissue heat transfer as if it all takes place in the capillaries: blood reaches the capillaries with the temperature still that of the major supply artery. In the capillaries thermal equilibration to the tissue temperature takes place, leading to the 'heatsink' term in Eq. (2.1). Subsequently, in the venous return system again all heat transfer with the tissue is assumed negligible. The bio heat equation has established itself as the most used continuum description of tissue heat transfer. The results can be quite accurate, especially in tissues that are highly perfused such as the brain. The cause for the better accuracy at higher perfusion is that in highly perfused tissue a relatively large *proportion* of the heat transfer does take place in the smallest vessels. To put it slightly differently, increasing blood flow in the branching vessel network will lead to later thermal equilibration of blood with tissue, further into the network, closer to the capillaries.

As an example of the use of the Pennes equation, the temperature difference between the blood going to the brain and the returning blood will be estimated. In the central brain, convective heat transfer by the blood is so dominant that conduction can be neglected. From Eq. (2.1), this means that in the stationary situation the metabolic heat production rate must equal $c_{\text{b}}W_{\text{b}}(T - T_{\text{art}})$. Using $c_{\text{b}} = 3.6\ \text{kJK}^{-1}\text{kg}^{-1}$, $W_{\text{b}} = 9\ \text{kg}\,\text{m}^{-3}\text{s}^{-1}$ and a metabolic heat production in the brain of $10\ \text{kWm}^{-3}$ this means that the temperature of the brain (and of the returning blood) is roughly 0.3°C higher than the temperature of the incoming blood.

As implied before, heat transfer between tissue and blood *does* take place before and after the capillaries. In fact, for the arterial blood it was demonstrated that by the time blood flows into vessels $60\,\mu$m in diameter and smaller the equilibration process is complete. On the one hand, this means that the effect of blood is not only dependent on the volumetric perfusion distribution $W_{\mathrm{b}}(\boldsymbol{r})$, but also on the positions of the large vessels of the vasculature. On the other hand, this leads to two possible additional terms in the continuum heat transfer equation. One is associated with the net mass flow of blood and was first proposed by Wulff [2] as a replacement for the heatsink term.

$$\rho_{\mathrm{tis}} c_{\mathrm{tis}} \frac{\partial T}{\partial t} = \boldsymbol{\nabla} \cdot k_{\mathrm{tis}} \boldsymbol{\nabla} T - c_{\mathrm{b}} \rho_{\mathrm{b}} \mathbf{U} \cdot \boldsymbol{\nabla} T + M$$

In this equation the convection term, in which $\mathbf{U}$ is the local mean apparent blood velocity $\left[\mathrm{m\,s^{-1}}\right]$, accounts completely for the effect of blood flow. In reality, significant unidirectional flow on meaningful length scales is rare in the body. The other possible additional term to the heat transfer equation is an increased tissue thermal conductivity. It was first introduced by Chen and Holmes in 1980, [3]. They proposed to model heat transfer from large vessels individually, to use the last individually calculated blood temperature T^*_{art} for the remaining heat sink term and to add two convective terms to the heatsink formulation:

$$\rho_{\mathrm{tis}} c_{\mathrm{tis}} \frac{\partial T}{\partial t} = \boldsymbol{\nabla} \cdot k_{\mathrm{tis}} \boldsymbol{\nabla} T - c_{\mathrm{b}} W_{\mathrm{b}} (T - T^*_{\mathrm{art}}) - \rho_{\mathrm{b}} c_{\mathrm{b}} \mathbf{U} \cdot \boldsymbol{\nabla} T + \boldsymbol{\nabla} \cdot k_p \boldsymbol{\nabla} T + M$$

The new perfusion based term, containing k_p, states that part of the effect of blood flow is qualitatively the same as an increase in thermal conductivity. The term arises from the net thermal effect of flow in vessels where the macroscopic net flow is zero because the flow in one vessel is matched by the same flow in the opposite direction in (an)other vessel(s). After it was observed that blood vessels often occur in countercurrent pairs, it was even suggested that just an increased effectivity, without heatsink, could describe the effect of blood flow in some tissues. Incomplete countercurrent heat exchange does indeed qualitatively behave as an extra conduction term. After anatomical and theoretical studies of peripheral muscle tissue Weinbaum and Jiji, [4], formulated a bio heat equation in which the thermal effect of blood was described solely by an effective conductivity tensor k_{eff}. The dependence of k_{eff} on the vasculature was derived for homogeneous tissue containing vessels

with radius r_{ves} as

$$k_p + k_{\text{tis}} = (k_{ij})_{\text{eff}} = k_{\text{tis}} \left(\delta_{ij} + \frac{\pi^2}{4\sigma\, k_{\text{tis}}^2} n\, r_{\text{ves}}^2\, k_{\text{b}} \text{Pe}^2 l_i l_j \right).$$

Here δ_{ij} is the Kronecker delta function, i and j are the directions of the heat flux and temperature gradient, σ is a shape factor (describing vessel-tissue heat transfer), n is the vessel pair density $\left[\text{m}^{-2}\right]$, and l_i, l_j are direction cosines. Pe is the Peclet number equal $2\rho_{\text{b}} c_{\text{b}} r_{\text{ves}} u_{\text{b}} / k_{\text{b}}$, in which u_{b} is the blood velocity $\left[\text{ms}^{-1}\right]$. This relation for k_{eff} does not quite show the complexities involved, and an alternative equation will be derived below.

2.2. Vessel Pairs and Effective Conductivity

It is worth taking a look at how a pair of countercurrent vessels contributes to the net heat flow. Consider a cross section of a tissue block with a vessel pair with equal but opposite flows, and a temperature gradient in the direction of the axis of the tissue cylinder. The contribution of the countercurrent vessel pair to heat transfer in the vessels' direction will both be proportional to the volume flow in the vessels, and to the temperature difference between the blood in the vessels. The difficulty lies with the second factor. The blood temperature difference depends on what has gone on before, not just on the local tissue temperature gradient. If the length scale of the gradient is sufficiently large, the temperature difference between the two vessels will be proportional to the gradient. Heat transfer proportional to gradient

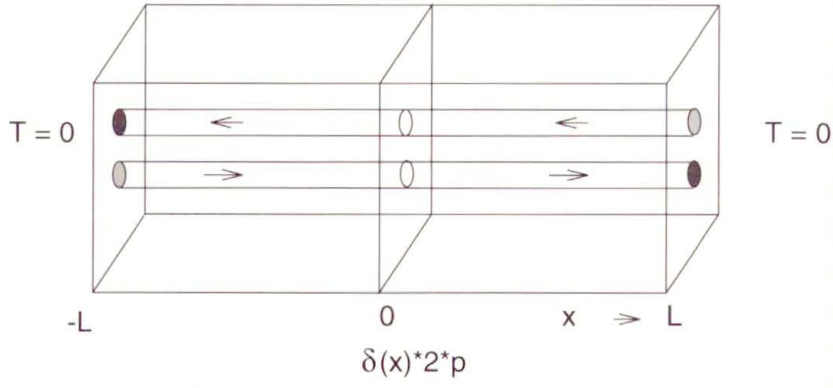

FIGURE 3. Two countercurrent vessels with same inflow temperature in a block with heating in central plane, with the four walls coplanar to the vessels thermally insulated, and the two faces at constant temperature.

means that in this case indeed the vessels contribute a term equivalent to Fourier's law for conduction. For the smallest vessels, that equilibrate quickly with the tissue, a short length scale of the gradient will suffice. This means that an effective conductivity description is often accurate for small vessels. However, because of the small flow and the small temperature difference between the vessels (because of same rapid equilibration) the contribution of the smallest vessels to the conductivity is small. For larger vessels a larger effective conductivity is possible, but the required large length scale for the gradient might not always be present, making the behaviour of the vessels qualitatively different, and possibly much more heatsink like.

A simple theoretical analysis of a countercurrent pair in tissue gives a quantitative but not completely rigorous description of this behaviour. A three-equation formulation reduces the complex 3-D temperature distribution to three axial profiles, [5]. One axial profile, $T(z)$, describes the tissue temperature as averaged over the tissue cross section. The other two profiles, $T_{\mathrm{art}}(z)$ and $T_{\mathrm{vein}}(z)$, describe the vessel mixing-cup temperatures (e.g. [6]) of the countercurrent vessels

$$T_{\mathrm{mix-cup}} \equiv \frac{\int_0^{r_{\mathrm{ves}}} T_{\mathrm{b}}(r) u_{\mathrm{b}}(r) 2\pi r \, \mathrm{d}r}{\int_0^{r_{\mathrm{ves}}} u_{\mathrm{b}}(r) 2\pi r \, \mathrm{d}r}.$$

The three governing differential equations can be written as

$$k_{\mathrm{tis}} \frac{\partial^2 T}{\partial z^2} - n k_{\mathrm{tis}} \sigma_{\Sigma} \left[T - \frac{T_{\mathrm{art}} + T_{\mathrm{vein}}}{2} \right] + M = \rho_{\mathrm{tis}} c_{\mathrm{tis}} \frac{\partial T}{\partial t}$$

$$\pi r_{\mathrm{ves}}^2 \rho_{\mathrm{b}} c_{\mathrm{b}} u_{\mathrm{b}} \frac{\mathrm{d}T_{\mathrm{art}}}{\mathrm{d}z} = -k_{\mathrm{tis}} \sigma_{\Delta} \left(T_{\mathrm{art}} - T_{\mathrm{vein}} \right) + \frac{k_{\mathrm{tis}} \sigma_{\Sigma}}{2} \left[T - \frac{T_{\mathrm{art}} + T_{\mathrm{vein}}}{2} \right] + \pi r_{\mathrm{ves}}^2 P$$

$$\pi r_{\mathrm{ves}}^2 \rho_{\mathrm{b}} c_{\mathrm{b}} u_{\mathrm{b}} \frac{\mathrm{d}T_{\mathrm{vein}}}{\mathrm{d}z} = -k_{\mathrm{tis}} \sigma_{\Delta} \left(T_{\mathrm{art}} - T_{\mathrm{vein}} \right) - \frac{k_{\mathrm{tis}} \sigma_{\Sigma}}{2} \left[T - \frac{T_{\mathrm{art}} + T_{\mathrm{vein}}}{2} \right] - \pi r_{\mathrm{ves}}^2 P$$

The mutual heat exchanges are calculated using the conduction coupling constants, or shape coefficients, σ_{Δ} and σ_{Σ}. The constant σ_{Δ} determines

the heat transfer between the vessels, σ_Σ determines the net heat transfer between vessel pair and tissue. The values of these coupling constants can be calculated on the basis of 2-D stationary temperature distributions. They only depend on the geometry (vessel size and spacing, tissue cross section), not on the flow in the vessels. $M(z)$ is the sum of metabolic heat and volumetric power absorption (e.g. from microwaves), $P(z)$ is absorbed power only as the metabolic rate in the blood is zero.

When a sinusoidal profile with arbitrary period $4L$ for the average tissue temperature is considered, it is easy to show that the solution for the sum of $T_{\mathrm{art}} + T_{\mathrm{vein}}$ is also a sinusoidal and in phase with $T(z)$. The difference $T_{\mathrm{art}} - T_{\mathrm{vein}}$ is also sinusoidal but is out of phase by $\pi/2$, so in phase with the tissue temperature gradient. From these solutions a relation for the effective conductivity can be worked out:

$$k_{\mathrm{eff}} = k_{\mathrm{tis}} \left(1 + \sqrt{\frac{\sigma_\Sigma}{\sigma_\Delta}} \frac{\mathrm{Pe}^* L_{\mathrm{cc}}^*}{1 + \pi^2 L_{\mathrm{cc}}^{*2}/4} \right),$$
$$\mathrm{Pe}^* \equiv \frac{\rho_{\mathrm{b}} c_{\mathrm{b}} L u_{\mathrm{b}} r_{\mathrm{ves}}^2}{k_{\mathrm{tis}} r_{\mathrm{tis}}^2}, \quad L_{\mathrm{cc}}^* = \frac{\pi \rho_{\mathrm{b}} c_{\mathrm{b}} u_{\mathrm{b}} r_{\mathrm{ves}}^2}{\sqrt{\sigma_\Sigma \sigma_\Delta} k_{\mathrm{tis}} L}. \tag{2.2}$$

Here Pe^* is a modified Peclet number, and L_{cc}^* is a dimensionless parameter describing the length of countercurrent thermal equilibration with respect to the length of the sine period. It can be seen that k_{eff} goes asymptotically to a maximum when L increases. When L goes to zero, the contribution of the vessels to the conductivity goes to zero. This is because for very small L the amplitude of the sinusoidal vessel temperatures will go to zero, resulting in a more heatsink-like effect of the vessels. One further thing to note about the relation 2.2 is that for small L_{cc}^* the extra conductivity is quadratic in the blood volume flow. In summary, large vessels can potentially contribute a lot to the effective conductivity, but this requires a gradient with a long length scale to build up the temperature difference. This is also illustrated in Fig. 4 where it is shown how two countercurrent vessels increase their share of the heat transport where the distance from the discontinuity increases. Tissue temperature gradients with small length scales, for instance in the case of interstitial heating with needles, will necessarily experience a relatively low effective conductivity.

The above analysis suggests that continuum models have non-trivial inherent limitations. Even homogeneously vascularised tissue may have spatially varying optimum continuum parameters, based on different distances

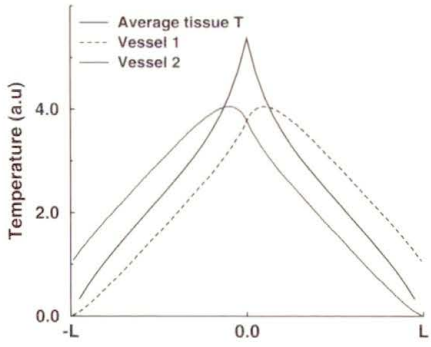

FIGURE 4. Profiles for two countercurrent vessel temperatures and average tissue temperature in tissue block with heating in central plane, see Fig. 3. The varying contribution of the vessels to the heat transport can be appraised from the variation in tissue temperature gradient.

with respect to the boundary conditions. May be as a result of this complex behaviour, there has been considerable debate in the past over the applicability of the different paradigms (heatsink, effective conductivity). These differences were difficult to resolve, because of inherent difficulties in experimental measurements, [7, 8], but also because different experimental set-ups may lead to different dominant behaviour. Now, however, there seems to be a somewhat better understanding of the limitations of each of the paradigms. This is partly thanks to the development and experiences with numerical models that describe the influence of individual blood vessels.

Even now increasingly powerful computers, sophisticated models, and imaging techniques, have made it possible to account for the thermal effects of individual vessels, there is still an important role for continuum models. Creating a detailed vasculature for an individual patient requires an enormous effort. For some applications the continuum models will be good enough not to make this effort. Even when discrete vessel modelling is applied, this will often not be possible for all of the thermally significant vessels, in which case the discrete vessel model is used in combination with a continuum description.

3. Discrete Vessel Thermal Model

It is obvious that one of the inherent disadvantages of all continuum models is that they don't account for temperature inhomogeneities surrounding

the large vessels, simply because these are not modelled. One field where one is very much interested in these inhomogeneities is that of treatment of tumours with local hyperthermia, [9]. Hyperthermia is the heating of tumours to about 43°C, not so much to directly kill tumour cells, but as an adjuvant therapy to make radiotherapy more effective. In local (rather than regional or whole-body) hyperthermia in particular, very heterogeneous temperature distributions may be brought about by arteries with normal blood temperature entering the heated volume. These temperature inhomogeneities may have serious consequences for the efficacy of the treatment. Therefore, especially in this field, the effects of individual vessels on the temperature distribution have been studied and increasingly sophisticated numerical models have been developed.

3.1. Analytic Solution for a Vessel in a Tissue Cylinder

It is instructive to first look at the analytical solution for the very simple geometry of one vessel embedded in a tissue cylinder, see Fig. 5. It introduces the important concept of thermal equilibration length, and results will be used later on in the discrete vessel thermal model. Consider a straight blood vessel in a concentric tissue cylinder with constant temperature on the outside cylindrical surface, constant conductivity k_{tis}, and no heat generation in the tissue. The governing differential equation in the tissue surrounding the vessel

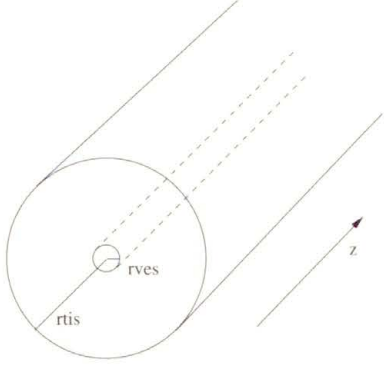

Figure 5. Geometry: a straight vessel in a tissue cylinder with constant boundary temperature

is written in cylindrical coordinates as

$$k_{\text{tis}}\left(\frac{\partial^2 T}{\partial r^2}+\frac{1}{r}\frac{\partial T}{\partial r}+\frac{1}{r^2}\frac{\partial^2 T}{\partial \theta^2}+\frac{\partial^2 T}{\partial z^2}\right)=\rho_{\text{tis}}c_{\text{tis}}\frac{\partial T}{\partial t}.$$

The solution to this problem is considerably simplified if it is assumed that conduction in the axial direction can be neglected. Furthermore, the stationary solution must be cylindrically symmetric because of the fixed temperature on the tissue boundary. So, what is left is a one-dimensional differential equation for the radial tissue temperature profile. The solution is given by

$$T(r)=T(r_{\text{ves}})+(T(r_{\text{tis}})-T(r_{\text{ves}}))\frac{\ln(r/r_{\text{ves}})}{\ln(r_{\text{tis}}/r_{\text{ves}})}.$$

The tissue temperature at the vessel wall is unknown, but can be found since the radial heat flux ϕ must be continuous over the vessel wall. The heat flux in the tissue at the vessel wall boundary can be calculated by

$$\phi_{w^+}=-k_{\text{tis}}\left.\frac{\mathrm{d}T}{\mathrm{d}r}\right|_{r_{\text{ves}}}=-k_{\text{tis}}\frac{T(r_{\text{tis}})-T(r_{\text{ves}})}{\ln(r_{\text{tis}}/r_{\text{ves}})r_{\text{ves}}}.$$

Inside the vessel, the heat flux at the wall can be written as

$$\phi_{w^-}=-\frac{1}{2r_{\text{ves}}}\,\text{Nu}\,k_{\text{b}}\,(T(r_{\text{ves}})-T_{\text{art}})\,. \tag{3.1}$$

The Nusselt number Nu is a dimensionless heat transfer coefficient, providing a measure for the heat transfer at a boundary of a flowing fluid. Here $\text{Nu}=hD/k_{\text{b}}$, where h is the convective heat transfer coefficient $\left[\text{Wm}^{-2}\text{K}^{-1}\right]$ defined by $h=\phi_{w^-}/(T_{\text{mix-cup}}-T_{\text{wall}})$ and D is the vessel diameter. For a number of cases, expressions for the Nusselt number have been derived. In a cylinder, for a Newtonian fluid with Poiseuille flow and thermally developed flow, $\text{Nu}=3.66$ if the wall temperature is constant along the vessel, whereas $\text{Nu}=4.36$ if instead the heat flux through the wall is constant, [6]. In this case, the presence of the tissue between vessel and the outer boundary with constant temperature causes the Nusselt number to fall between these two values. However, for thermally undeveloped flow Nu may be higher than both.

From the continuity requirement for the radial heat flux through the wall, the wall temperature is found to be

$$T(r_{\text{ves}})=T_{\text{art}}+\frac{T(r_{\text{tis}})-T_{\text{art}}}{1+\frac{1}{2}\text{Nu}\frac{k_{\text{b}}}{k_{\text{tis}}}\ln\frac{r_{\text{tis}}}{r_{\text{ves}}}}\,.$$

Substitution in Eq. (3.1) gives an expression for the heat flux into the vessel. This heat flux causes the blood temperature to change along the vessel direction, and the axial profile for the vessel temperature can now be determined from the differential equation:

$$\pi r_{\mathrm{ves}}^2 u_{\mathrm{b}} \rho_{\mathrm{b}} c_{\mathrm{b}} \frac{\mathrm{d}T_{\mathrm{art}}}{\mathrm{d}z} = 2\pi r_{\mathrm{ves}} \phi_w = \pi \mathrm{Nu}\, k_{\mathrm{b}} \frac{T(r_{\mathrm{tis}}) - T_{\mathrm{art}}}{1 + \frac{1}{2}\mathrm{Nu}\frac{k_{\mathrm{b}}}{k_{\mathrm{tis}}} \ln \frac{r_{\mathrm{tis}}}{r_{\mathrm{ves}}}} \,. \tag{3.2}$$

The solution is:

$$\begin{aligned} T_{\mathrm{art}}(z) &= T(r_{\mathrm{tis}}) + (T_{\mathrm{art}}(0) - T(r_{\mathrm{tis}}))\, e^{-z/L_{\mathrm{eq}}} \,, \\ L_{\mathrm{eq}} &= \rho_{\mathrm{b}} c_{\mathrm{b}} u_{\mathrm{b}} r_{\mathrm{ves}}^2 \left(\frac{1}{k_{\mathrm{b}} \mathrm{Nu}} + \frac{1}{2k_{\mathrm{tis}}} \ln \frac{r_{\mathrm{tis}}}{r_{\mathrm{ves}}} \right) . \end{aligned} \tag{3.3}$$

The thermal equilibration length L_{eq} describes the rate of thermal equilibration of the blood to the surrounding tissue. Clearly, the thermal equilibration length varies very strongly with varying radius. There is an explicit quadratic dependence of L_{eq} on vessel radius in Eq. (3.3), but in addition the flow velocity u_{b} will usually also be larger in a larger vessel. For several sizes of vessels approximate equilibation lengths have been tabulated in Table 1. From this table it can be deduced that most of the thermal equilibration must take place in the arteries with diameters in the range 0.2–2.0 mm. Note that because of branching the total surface area increases for every generation of smaller vessels.

TABLE 1. Equilibration length calculated for blood vessels of different sizes. Calculated assuming the vessel influences a tissue cylinder ten times larger than the vessel, [10].

vessel type	diameter mm	length cm	u_{b} cm/s	L_{eq} cm
aorta	25	40	100	1.5×10^5
large arteries	3	20	13	290
main branches	1	10	8	20
secondary branches	0.6	4	8	7.2
tertiary branches	0.14	1.4	3.4	0.17
terminal branches	0.05	0.1	2	0.013
arterioles	0.02	0.2	0.3	0.0003
capillaries	0.008	0.1	0.07	0.00001

3.2. Numerical Modelling of Detailed Vessel Networks

The impact of blood vessels on the temperature distribution can be calculated analytically only for very basic configurations. The modelling of the thermal impact of a complex, detailed discrete vasculature has to be done numerically.

In this text the computer progam DIVA, [11] (for DIscrete VAsculature) developed at the Utrecht University Medical Centre will be discussed in some detail. This program is unique in some important aspects, but shares essential properties with other models. Key of most models is that to be able to handle detailed vasculature the blood radial temperature profile is just described by the blood mixing-cup temperature. An analytical solution is used to describe vessel-tissue heat transfer. Unique for DIVA is that the vessels are described independently from the solid tissue: tissue and vessel do share the same coordinate system but are described by separate structures, in separate files. Whereas the tissue anatomy is described on a regular rectangular grid, the blood vessels are described as geometrical, curved tracks in 3-D with associated diameter and blood flow. So, for example, it is possible to change the resolution of one independent of the other.

When DIVA is employed to calculate a tissue temperature distribution including effects of discrete vessels, DIVA starts with an initialization routine. In this, possibly lengthy, initialization the relative positions of all the vessels with respect to the tissue are evaluated. For each elementary vessel part, two sets of voxels (volume elements) in the tissue are determined, see Fig. 6. One set consists of the tissue voxels that are located immediately surrounding

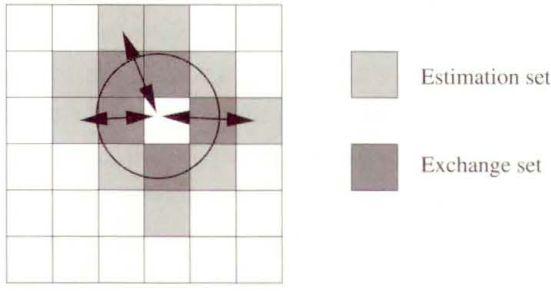

FIGURE 6. A piece of tissue layer with a vessel passing through in perpendicular direction. Dynamically determined estimation set voxels (light grey) and exchange set voxels (dark grey) have been drawn. Arrows show distances from vessel centre to estimation voxels as used in the calculation of the heat flow rates.

the vessel. These voxels are the so-called estimation set voxels, they are used in determining the heat flux between vessel element and tissue. The second set of voxels, named exchange set voxels, are tissue voxels that are within the vessel element and that border estimation set voxels. In these voxels the computed heat exchange between vessel and tissue is accounted for in the tissue. The vessel shown in Fig. 6 happens to be larger than voxel-size. A vessel can alternatively be small compared to the voxels. In that case, to guarantee a non-empty exchange set, the voxels along the vessel centre-line will be included in the exchange set, irrespective of whether the voxel centre is located within the vessel or not. For each such exchange set voxel, the four surrounding voxels will be included in the estimation set.

For the calculation of the time evolution of the temperature in the tissue DIVA uses a finite-difference scheme. The heat exchange between vessels and tissue is calculated using the estimation set. For each of the estimation set voxels, the heat flux at the vessel wall is determined using the analytical solution developed in Sec. 3.1. Each heat flux estimate is based on the tissue node temperature and the exact distance from vessel centre-line to specific tissue voxel centre. The local heat fluxes are calculated using the right part of Eq. (3.2), assuming the local heat flux is the same as if the temperature distribution immediately around the vessel were cylinder symmetric. Every estimation set voxel thus yields an estimate for the flux, and if the temperature distribution is indeed close to cylinder symmetrical the heat flux estimates will be quite close. The heat fluxes are subsequently averaged and multiplied by the vessel element wall area to result in the rate of heat exchange. When multiplied by the time-step the heat exchanged in one iteration is found. In the tissue this exchanged heat is equally distributed over the exchange set voxels associated with the vessel element. As such, the exchange set voxels will not have a temperature that corresponds to an actual temperature. Rather, these voxels that underlie vessel elements have a temperature that makes the heat exchange correct. Detailed testing has shown that the method gives accurate results, even if the temperature distribution around the vessels is quite different from cylindrically symmetric, [12].

The heat exchange must also be accounted for in the vessel. First, DIVA calculates the temperature rise from the heat exchange and the heat capacity of the volume of blood within the vessel element:

$$\Delta T_{\mathrm{bl}} = \frac{\langle \phi_w \rangle 2\pi r_{\mathrm{ves}} \Delta s \Delta t}{\pi r_{\mathrm{ves}}^2 \Delta s \rho_{\mathrm{b}} c_{\mathrm{b}}}$$

Here $\langle \phi_w \rangle$ is the averaged heat flux, and Δs is the length along the vessel element. After adding the respective temperature changes to the temperatures of all the vessel elements that make up the vessel, the next step is to account for the flow of the blood. This is done by shifting the axial temperature profile the appropriate amount for the time-step, and then interpolating the profile to get the new temperatures at the locations of the vessel element centres. For short equilibration lengths, heat fluxes will change rapidly along the length of the vessels. To minimize discretisation errors, in actual fact DIVA interpolates radial heat fluxes between consecutive vessel elements based on the path length traveled.

The vasculature in a real tissue block forms a branching network. DIVA models this as collections of connected vessel segments that form either arterial or venous vessel 'trees', see Fig. 7. In an arterial tree the flow is in the direction of the branching; in a venous tree the flow is in the opposite direction. The volume flows in the vessel segments can be individually set in

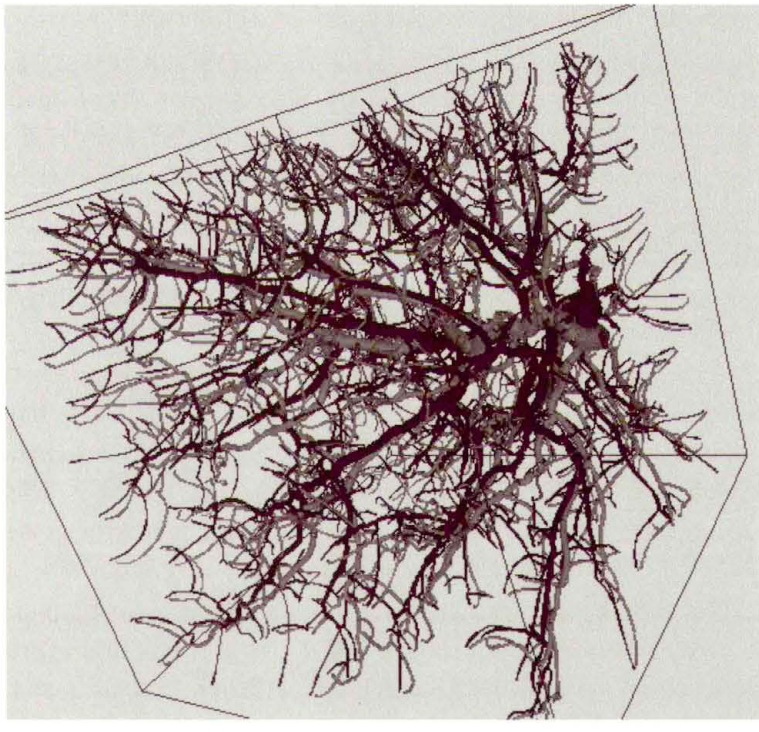

FIGURE 7. Detailed computer-generated arterial and venous vessel trees employed in numerical studies using the DIVA thermal model, [13].

the vessel tree description file. DIVA allows that the sum of the flows in the daughter branches is not equal to the flow in the parent branch. It is indeed desirable that conservation of flow is not guaranteed, as flow lost to vessels that are too small to be modelled discretely can be accounted for this way.

At some point, arterial blood in the model will flow out off the discrete vessel structure. Either at the end of a terminal vessel, or as bleed-off at a branch-point. In clinical practice it is difficult to obtain a detailed description of a patient's vasculature, so this point may be sooner rather than later. In reality the blood will flow in smaller vessels that may still have a (very) signicant thermal effect. It may be the case that the blood as it reaches the end of the terminal branches is still far from thermally equilibrated with the surrounding tissue. In that case, the most obvious way forward is to use the Pennes heatsink Eq. (2.1). Naturally, the individual outflow temperatures of the terminal branches are substituted for T_{art} in the heatsink term. It is less obvious *where* the heatsink with this temperature should be applied. There could be very many different terminal branches, with quite different outflow temperatures. Or, for a rather rudimentary vessel network, there could be just a few branches with outflow points that have a very poor correspondence to the actual perfusion distribution. DIVA has several ways of dealing with the outflow. If the discrete vessel network is very detailed, the density of terminal branches may be a reasonable match of the perfusion distribution in the tissue. For that case, the DIVA model offers the possibility of assigning volumes to every branch. These volumes, which might be spheres but can also be different, are assumed to be the tissue volumes that are supplied by blood from the vessel branch in question. From the mass flow in the terminal vessel and the volume of the tissue where the local heatsink is applied, the local perfusion in the affected voxels realised by the branch can be calculated. The heatsink term can now be applied in the tissue. It must be noted that some voxels may receive blood from more than one source, whereas other voxels may not receive any blood at all. Serious artefacts can occur because of this, especially for discrete vasculatures consisting just of a few main branches. In that case it is more appropriate to calculate the average temperature of the blood over all terminating arteries and use this one temperature for the whole tissue volume, together with the local perfusion, to calculate the local heat sink term.

So far, there has been not much mention of the dynamics of the important parameters that govern the heat transfer. Tissue physical properties such as

thermal conductivity are dependent on temperature. Often these variations are neglected, but care should be taken when temperature changes a lot. It should be obvious that change in tissue parameters will be highly significant if heat is used for tissue ablation. Blood flow will also vary under varying circumstances. Blood flow, however, is not just determined by local temperature, but is dependent on temperatures at other body sites too. This will be discussed in greater detail in Sec. 5.2.

Varying the tissue and blood flow parameters does not conceptually make a difference to the thermal model. It aims to follow the time evolution of the temperature distribution, so if the temperature dependencies are known, the information is available to change properties as appropiate each timestep. In practice, it can make the modelling quite a bit more cumbersome.

4. Application: the Temperature Rise Caused by a Mobile Phone

To demonstrate the many aspects that play a role in predicting tissue temperatures including the effects of discrete vessels, as an example the calculation of the rise in temperature caused by a mobile phone will be described. The motivation for this study, [14] were safety concerns over the effect on the brain of the electromagnetic radiation transmitted by a mobile phone's antenna. Safety regulations for the GSM900 frequency band, 880–915 MHz, were based on the thermal effects, but the relation between absorbed power and temperature had not been precisely studied before. Experimental studies have severe limitations; this numerical study set out to compute both power and temperature for a typical adult head.

First, a detailed description of the anatomy had to be obtained. For both the electromagnetic computations and temperature computations a detailed 3-D distribution of physical properties was necessary. For the temperature computations in addition a detailed description of the vasculature was needed, of which the relative positions with respect to the tissue should be known. To obtain the vasculature, phase-contrast Magnetic Resonance Angiography (MRA) scans were made of the head of a volunteer. A characteristic of this MRA technique is that it, as part of the procedure, acquires T_1-weighted MR images which give information about the solid tissue. These 3-D MR intensity images were used to create a 3-D tissue type distribution using computer-aided segmentation. Because the different tissue types

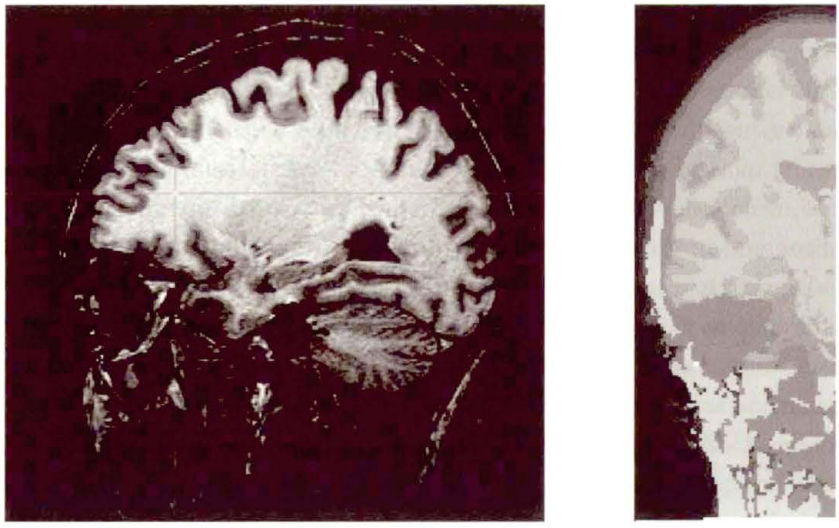

FIGURE 8. Left: a sagittal slice (through an eye) of the original MR data; right: a coronal slice through the segmented 3-D head.

did not have exclusive ranges of MR image values, the segmentation had to be done partially by hand, especially in the thin superficial layers. Distinguished tissue types were, a.o., skin, fat, bone, brain grey matter, white matter, CSF, and muscle. The required distribution of physical properties was now available through a look-up table relating local tissue type with required property. The discrete vasculature was interactively built, tracing the visible vessels in the 3-D MRA images. The result of the tracking was six wireframe skeletons representing vascular trees. These were still rather crude, with smallest diameters approximately 0.7 mm. The appropriate flow directions were determined from an anatomical atlas. Next, corresponding to the different perfusions of the tissue types in the head, smaller vessels were added to these tracked vessels quasi at random. The rationale was that this would best mimic the behaviour of the vascularized tissue; even if the exact locations of the smallest vessels are not correct. For the aim of this study, the statistics of the temperature distribution were far more interesting than the exact locations of the temperature. But also in developing a hyperthermia treatment plan for a specific patient, this 'additional generic vasculature' approach is interesting as it offers the best possible temperature predictions—at the cost of extra computation time.

The electromagnetic power density distribution in the head caused by

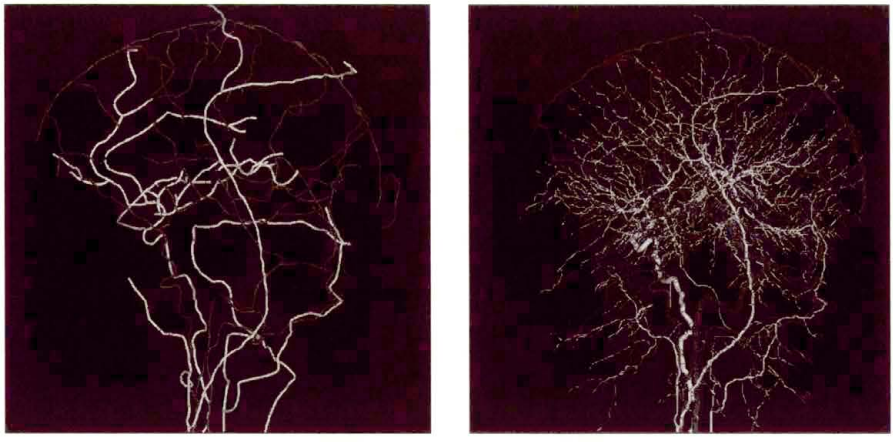

FIGURE 9. Left: a view of the manually tracked vessels. Right: the vasculature including computer generated smaller vessels.

the transmitting dipole antenna was calculated using the finite-difference time domain (FDTD) method. Thermal simulations with the DIVA model determined the stationary temperature distributions in the head with and without operating antenna. Air in the DIVA model (ambient and in the nasal passage) can not flow. The convective and radiative heat transfer from the skin was modelled by fixing the temperature of the air voxels and adjusting the thermal conductivity to the voxel size such that in effect a heat transfer coefficient between skin surface and air of $8\,\mathrm{W\,K^{-1}\,m^{-2}}$ was modelled.

The typical maximum average output of a mobile phone is 0.25 W. For this power, the highest SAR (Specific Absorption Rate) in a 10 g cube of tissue was $0.91\,\mathrm{W\,kg^{-1}}$. Because of the different electromagnetic properties of the tissues the EM power absorption does not monotonically decrease with depth, but is higher in the brain than in skull. The temperature distributions with and without power were first calculated for a whole head using the Pennes heatsink equation. Then high resolution ($(1\ \mathrm{mm})^3$ voxels) temperature simulations for the region of interest were done with DIVA and the discrete vasculature, with boundary conditions determined by the heatsink simulations. Because of thermal conduction the temperature rise distribution is much smoother than the EM absorption distribution. The maximum rise caused by the EM absorption is highest in the skin at 0.16°C, and the maximum rise in the brain is 0.11°C.

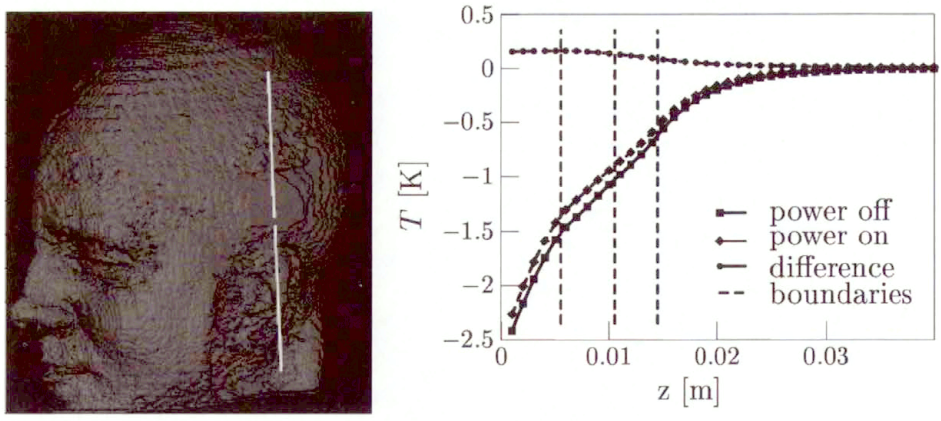

Figure 10. Left: the model antenna at its modelled position with respect to the head. Right: the temperature rise caused by the absorbed power, and temperature profiles with, and without power ($T_{\text{art}} \equiv 0$).

5. Whole-body Models, Human Thermoregulation

5.1. Introduction

The human body, when healthy, maintains a core temperature of about 37°C with only small deviations. The core consists of the brain and the internal organs in the trunk, see Fig. 11. Temperatures in the remaining parts of the body—'the periphery': surface tissue and the limbs—are much less constant. The core temperature is maintained even though the environmental conditions can vary a lot. This is done partly by behaviour (e.g. clothing, drinking cold or hot liquids), and partly by the body's thermoregulatory system. Sweating and shivering are easily perceptible themoregulatory reactions in warm and cold environments respectively. Less perceptible but just as important are changes in blood flow. By increasing or reducing blood flow to the skin, the body can increase or lower the skin temperature and hence its heat transfer to the environment.

There are many parameters that have an influence on the temperature distribution. Heat transfer to the environment through radiation, convection, conduction and evaporation, depend on wall temperatures, ambient temperature distribution, air speed relative to body parts, vapour pressure in air, the sweat response, evaporative and conductive heat resistance of clothing, heat capacities, conductivities, and temperatures of objects in contact, the

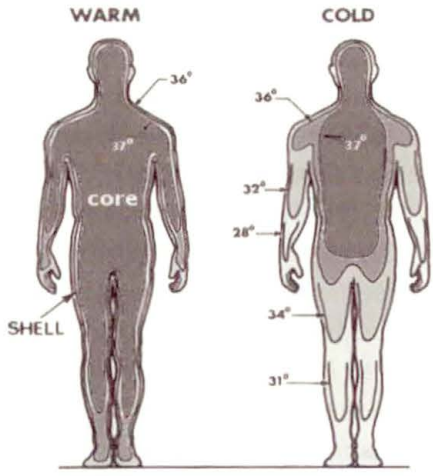

FIGURE 11. The human body can be thought of as consisting of an isothermal core and a periphery with variable temperature.

strength of the sun, etc. Heat production depends on activity level, body weight and composition, local tissue temperatures, shiver response, food intake, drugs, individual differences, illness, sleep deprivation, etc. Heat transfer within the body depends on sizes and locations of blood vessels in all of the body, blood volume flows, the tissue thermal properties, etc.

The applicability of a mathematical model for the calculation of whole-body temperature distributions depends on the precision with which all of the above are described.

First a few words on the biology of thermoregulation. The temperature of the human body is controlled in the hypothalamus. The hypothalamus receives temperature information from temperature receptors in the skin and mucous membranes, and from internal structures, which include the hypothalamus itself. The hypothalamic thermostat works together with other hypothalamic, autonomic and higher nervous thermoregulatory centers to keep the core temperature constant. Some of these thermoregulatory responses are involuntary, passed on by the autonomic nervous system, some are neurohormonal and others are semi-voluntary or voluntary behavioral responses. How exactly the cold and warm thresholds for action are determined is unknown. There is a daily variation, and also influences such as menstrual cycle, food intake, infection, and drugs can vary the thresholds. The difference between the warm and cold thresholds is called the interthreshold range, and this range is typically 0.4°C. The thermoregulatory responses kick in outside

the interthreshold range. Responses can influence either the amount of heat produced by the body, or the rate of heat transfer to the environment.

Low-cost thermoregulatory responses are applied before more costly (in terms of energy, water, minerals) responses. It is relatively inexpensive to decrease or increase blood flow to the skin in order to reduce or enlarge heat transfer from the body to the environment. Hence, vasoaction is used earlier than shivering and sweating. By vasoconstriction or vasodilatation the blood flow to the superficial capillaries can be varied between just over 0% to close to 30% of cardiac output. In a hot environment, sweating is extremely important. Even if the ambient temperature is higher than the body temperature, the body might still transfer heat to the surroundings by sweating if the humidity is not too high. For an adult, the maximum rate of sweating may lie between 10 and 15 liters in 6 hours. Alternatively, in a cold environment the amount of heat produced by the body may be increased by shivering. This uncontrolled muscle action can double or even more than quadruple the total metabolic rate. Non-shivering thermogenesis does also exist in humans, but looses its significance when growing up.

5.2. Mathematical Modelling

Several models have been developed to describe whole-body heat transfer, from just two nodes describing the core and the periphery (e.g. [15]) to multi-segment, multi-layered models. Many of the aspects and their complexities that play a role in accurate modelling of body temperature will be examined here by means of a discussion of the model developed by Dusan Fiala, [16, 17].

5.2.1. Anatomy of the Passive System Two node models may be useful in a somewhat narrow range of simple boundary conditions, and where only core temperature and skin temperature are needed. Typical application of these models is the evaluation of thermal comfort, [18]. To model a wider range of conditions a more detailed description of the anatomy must be used. The anatomy in the model published by Fiala in 1999 was built from ten elements, refining the earlier six segment model by Stolwijk, [19]. The elements describe head, face, neck, thorax, abdomen, shoulders, arms, hands, legs, feet, see Fig. 12. The back of the head is modelled as part of a sphere, all the other elements are cylindrical. Each of the elements consists of concentric layers of different tissue. The different tissue types in the anatomy are brain,

lung, bone, muscle, fat, skin and viscera. Each layer may be divided in several nodes in the radial direction, with a higher density of nodes in the outer layers. Most elements are also divided in several sectors, typically posterior, anterior and inferior, to be able to model inhomogeneous boundary conditions (e.g. smaller radiation view factors for inferior legs). There are no subdivisions in the axial direction. Each element is described by its physical dimensions, the layer thicknesses, and for each layer the tissue properties k_{tis}, ρ_{tis} and c_{tis}, the basal perfusion W_{b}, and the basal metabolic rate q_m.

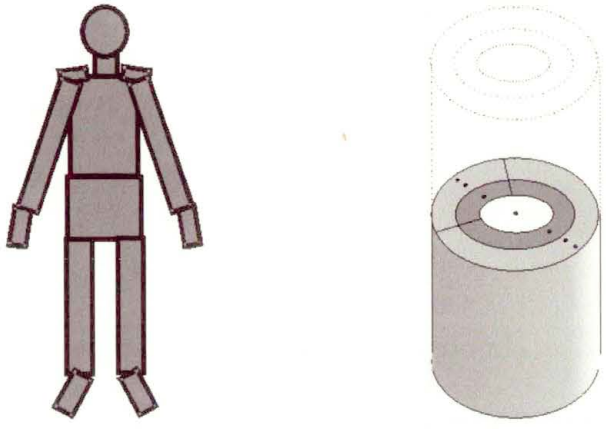

FIGURE 12. Schematic representation of the model anatomy. The model is built from cylinders and a sphere for the head (left); the elements are divided in concentric layers, the layers, apart from the core, are divided in sectors (right).

The model anatomy has the length, weight and body composition of an average man. By scaling the dimensions and varying the fat layer also different body types may be modelled. In many ways the anatomy is crude. A cross section through any of the real body parts would look quite a bit different. This goes especially for the two hands which are modelled as one cylinder with length 62 cm and radius 2.26 cm. However, the crude anatomy need not be a problem for the aims of this model. If the different volumes of tissue in the elements, and the surface areas for the elements are correct, both heat production and heat loss may be accurately predicted. The exact locations of the bones in the element won't matter a great deal. On the other hand, an accurate representation of the superficial layers is very important. In the model, the skin has two layers. The inner skin models the cutaneous plexus, where perfusion takes place and metabolic heat is generated. The perfusion in

the inner skin can change a lot under the influence of the thermoregulation. In the outer skin no perfusion or metabolic rate is modelled.

Within the tissue, heat transfer is modelled using the Pennes bioheat equation discussed before, in the appropriate coordinate systems:

$$\rho_{\mathrm{tis}} c_{\mathrm{tis}} \frac{\partial T}{\partial t} = k_{\mathrm{tis}} \left(\frac{\partial^2 T}{\partial r^2} + \frac{\omega}{r} \frac{\partial T}{\partial r} \right) - c_{\mathrm{b}} W_{\mathrm{b}} (T - T_{\mathrm{art}}) + M$$

with $\omega = 1$ for cylindrical coordinates and $\omega = 2$ for spherical coordinates. There is no axial conduction component as all the elements have only one node in the axial direction, and conduction between neighbouring elements is not modelled. In reality, under normal conditions, temperature gradients in the axial direction will be small, so this simplification has not much impact. The arterial temperature T_{art} is the temperature of the blood after countercurrent heat exchange. The method to solve the temperatures is by using a finite-difference scheme to discretize the bioheat equation.

Heat exchange between the blood in afferent arteries and in efferent veins on the way from heart to tissue and vice versa is modelled using countercurrent heat exchange coefficients (Fig. 13):

$$\Phi_{\mathrm{ccx}} = h_{\mathrm{x}} \left(T_{\mathrm{art}} - T_{\mathrm{vein}} \right). \tag{5.1}$$

Here, Φ_{ccx} is the total heat exchange beteen the vessels [W], h_{x} is the countercurrent heat exchange coefficient $\left[\mathrm{WK}^{-1}\right]$, T_{art} is the arterial blood tempera-

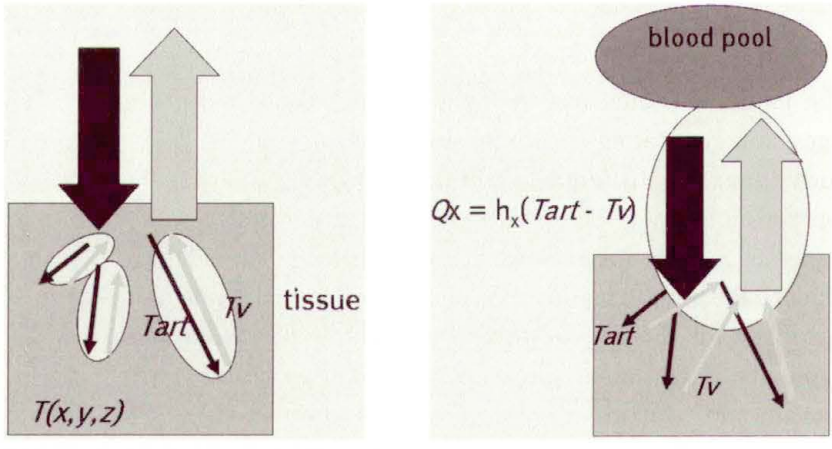

Figure 13. Conceptual difference between the local effective conductivity, Eq. (2.2)(cf. highlighted ellipsoids in left figure), and the countercurrent heat exchange coefficient for an element, Eq. (5.1) (highlighted ellipsoid right).

ture after countercurrent heat exchange and T_{vein} is the venous temperature before countercurrent heat exchange. It must be noted that all of the elements have their own countercurrent heat exchange coefficient, large for the hands and feet and zero for head, thorax and abdomen. Values for the coefficients were estimated by a trial-and-error procedure in which simulated local skin temperatures were made to match experimental values. The heat exchange causes a temperature change according to

$$T_{\text{bp}} - T_{\text{art}} = \frac{\Phi_{\text{ccx}}}{\dot{m}_b c_{\text{b}}} = \frac{h_x (T_{\text{art}} - T_{\text{vein}})}{\dot{m}_b c_{\text{b}}} \tag{5.2}$$

with T_{bp} the temperature of the blood pool, i.e. the temperature of the blood as it is in the heart. Directly from Eq. (5.2), for the temperature of the blood in the arteries reaching the tissue we have

$$T_{\text{art}} = \left(\frac{C}{C + h_x} \right) T_{\text{bp}} + \left(\frac{h_x}{C + h_x} \right) T_{\text{vein}}$$

with C the 'capacity rate' of the blood, defined as:

$$C = \dot{m}_b c_{\text{b}} = \rho_{\text{b}} c_{\text{b}} \int W_{\text{b}} \, \mathrm{d}V.$$

The venous temperature T_{vein} before countercurrent heat exchange is equal to the perfusion averaged temperature of the tissue in the element. This befits the Pennes bioheat equation, as it implies there is no heat exchange between veins and tissue

$$T_{\text{vein}} = \frac{\int W_{\text{b}} T \, \mathrm{d}V}{\int W_{\text{b}} \, \mathrm{d}V} \, .$$

The central bloodpool temperature T_{bp} is every time step calculated as the mixing-cup average temperature over all the elements of the venous blood flows after countercurrent heat exchange. This means there is no heat storage in the blood pool. The venous return temperatures are given by

$$T_{\text{vein,ccx}} = \left(\frac{C}{C + h_x} \right) T_{\text{vein}} + \left(\frac{h_x}{C + h_x} \right) T_{\text{bp}} \, .$$

Solving for the blood pool temperature:

$$
\begin{aligned}
T_{\mathrm{bp}} &= \frac{\sum_{\mathrm{i}} T_{\mathrm{vein,ccx,i}} C_{\mathrm{i}}}{\sum_{\mathrm{i}} C_{\mathrm{i}}} \\
\Rightarrow T_{\mathrm{bp}} &= \frac{\sum_{\mathrm{i}} \left[\left(\frac{C_{\mathrm{i}}}{C_{\mathrm{i}}+h_{x,i}} \right) T_{\mathrm{vein}} + \left(\frac{h_{x,i}}{C_{\mathrm{i}}+h_{x,i}} \right) T_{\mathrm{bp}} \right] C_{\mathrm{i}}}{\sum_{\mathrm{i}} C_{\mathrm{i}}} \\
\Rightarrow T_{\mathrm{bp}} &= \frac{\sum_{\mathrm{i}} \left(\frac{C_{\mathrm{i}}}{C_{\mathrm{i}}+h_{x,i}} \right) \int_{V_i} W_{\mathrm{b}} T \, \mathrm{d}V}{\sum_{\mathrm{i}} \left(\frac{C_{\mathrm{i}}}{C_{\mathrm{i}}+h_{x,i}} \right) \int_{V_i} W_{\mathrm{b}} \, \mathrm{d}V}
\end{aligned}
\tag{5.3}
$$

with C_{i} the capacity rates for the respective elements. From Eq. (5.3) the blood pool temperature can be calculated from the tissue temperatures.

The metabolic heat production in the tissue is the sum of the basal value q_m and additional terms that may be caused by the local thermoregulation, shivering (part of the global thermoregulation), and exercise. The basal metabolism of the total standard anatomy turns out to be 87 W, which is commensurate with measurements. The metabolism will change if the body is no longer in the thermal neutral situation. For all tissues in the model, the basal metabolic rate varies according to the Q_{10} effect describing the dependence of biological reactions on local tissue temperature

$$
q_{\mathrm{m,bas}} = q_{\mathrm{m,bas,0}} \times 2^{(T-T_0)/10^{\circ}\mathrm{C}} \, .
$$

If work is being done by the modelled subject, extra heat is generated. In the model, activity level in met (1 met$\equiv 58.2\,\mathrm{Wm}^{-2}$) is supplied as input to calculate the actual metabolic heat production. Activity level is a measure of the total power generated by the subject. For a reclining resting person the activity is 0.8 met. Confusingly, next to the unit 'met', used mainly by engineers, there is also the unit 'METS', used by physiologists, with 1 METS = 3.5 ml oxygen consumption per kg body mass per minute. There is no fixed conversion constant between the two units; for an average man 1 met is roughly 1.25 METS. When work is done on the outside world, this is done with an efficiency that varies but is never much more than 25%. The remainder of the power used goes into heating the muscles. In the Fiala model, the efficiency with which work is done is calculated from the activity level based on

regression analysis. The resulting heat production is divided over the muscle tissue according to the appropriate distribution coefficients for the type of work. Fiala gives two sets of work distribution factors: for standing and for seated work. Of course dedicated distribution factors for specific activities might be used if these are known.

5.2.2. Heat Exchange with the Environment Heat exchange with the environment takes place at the skin, and in the lungs/respiratory tract. The heat exchange by convection between skin surface at T_{sf} and ambient air T_{air} is described by a combined convection coefficient that considers both natural and forced convection

$$\phi_{\mathrm{c}} = h_{\mathrm{c,mix}} \times (T_{\mathrm{sf}} - T_{\mathrm{air}}) \,. \tag{5.4}$$

The $h_{\mathrm{c,mix}}$ are dependent on body location, and on the temperature difference between the surface and air, and the effective airspeed $v_{\mathrm{air,eff}}$.

$$h_{\mathrm{c,mix}} = \sqrt{a_{\mathrm{nat}} \sqrt{T_{\mathrm{sf}} - T_{\mathrm{air}}} + a_{\mathrm{frc}} v_{\mathrm{air,eff}} + a_{\mathrm{mix}}} \,.$$

The coefficients $a_{\mathrm{nat}}, a_{\mathrm{frc}}$ and a_{mix} are different for each element and were obtained from regression analysis of experiments in which local convective heat losses were measured for a heated full-scale manikin. Note that the convective heat transfer does not linearly depend on the temperatures, but that using the linearization in Eq. (5.4) will make it possible to solve for the temperatures using linear algebra. For the standard body, the mean convection coefficient is just over $3\,\mathrm{Wm^{-2}K^{-1}}$ for a temperature difference of 7°C between surface and air for all body elements. With a body surface area of $1.86\,\mathrm{m^2}$ this rather small difference corresponds to a convective heat loss of about 40 W for the nude body. For a temperature difference of 10°C the convection coefficient increases to about $4.2\,\mathrm{Wm^{-2}K^{-1}}$, leading to a convective loss of nearly 80 W, almost the total metabolic heat production in rest.

Heat exchange through radiation in the infra-red part of the electromagnetic spectrum, ϕ_{rad}, see Fig. 14, depends on the temperature difference between skin surface and surrounding walls. This is because air is almost completely transparent for infrared radiation. The equation describing radiative heat transfer between two infinite parallel surfaces, one at T_{sf} and the other at T_{wall} is

$$\phi_{\mathrm{r}} = \sigma \frac{T_{\mathrm{sf}}^4 - T_{\mathrm{wall}}^4}{\frac{1}{\epsilon_{\mathrm{sf}}} + \frac{1}{\epsilon_{\mathrm{wall}}} - 1}$$

Figure 14. Emitted infra-red radiation can be captured and used to visualize surface temperature.

where $\sigma = 5.6710^{-8}\mathrm{Wm}^{-2}\mathrm{K}^{-2}$ is the Boltzmann constant, and ϵ_{sf} and ϵ_{wall} are the emission coefficient of the object and the opposing wall. The temperatures are the absolute temperatures in Kelvin. Calculation of the radiative heat transfer for different skin sectors of the body requires accounting for the geometry. In the Fiala model this is done by different view factors and introduction of $T_{\mathrm{sr,m}}$ the mean temperature of the surrounding surfaces. The value of $T_{\mathrm{sr,m}}$ is defined as the temperature of a fictitious uniform envelope "seen" by the body sector, which causes the same radiative heat exchange as the actual surroundings. This was linearised as:

$$\begin{aligned} \phi_{\mathrm{r}} &= h_{\mathrm{r}} \times (T_{\mathrm{sf}} - T_{\mathrm{sr,m}}) , \\ h_{\mathrm{r}} &= \sigma \epsilon_{\mathrm{sf}} \epsilon_{\mathrm{sr,m}} \psi_{\mathrm{sf-sr,m}} \left(T_{\mathrm{sf}}^2 + T_{\mathrm{sr,m}}^2\right) (T_{\mathrm{sf}} + T_{\mathrm{sr,m}}) . \end{aligned}$$

with $\psi_{\mathrm{sf-sr,m}}$ the view factor for the sector. The view factors vary from 0.1 to unity. They were determined on the basis of how much individual skin sectors are concealed from the surrounding walls by other body parts. Sets of view factors have been calculated for different body postures. The ratio of the effective radiant area to the real area is 0.80 for standing and 0.74 for the seated standard body. The emissivity of the skin is 0.99, that of the surroundings typically 0.93 indoors.

It is possible that there is significant heat transfer from irradiation by the sun or other high temperature sources. This can be modelled in the skin sectors by terms

$$\phi_{\mathrm{sR}} = \alpha_{\mathrm{sf}} \psi_{\mathrm{sf-sr}} \, s$$

with α_{sf} the surface absorption coefficient, s $\left[\mathrm{Wm}^{-2}\right]$ the radiant intensity, and $\psi_{\mathrm{sf-sr}}$ the view factor between the skin sector and the surrounding envelope.

Even without thermoregulatory sweat response, there can be heat loss from the skin due to evaporation, caused by the vapour pressure in the skin being higher than in the ambient air. The heat loss caused by this spontaneous evaporation is determined by the skin moisture permeability and the evaporative coefficient at the skin surface. The former, alternatively written as a resistance $1/R_{\mathrm{e,sk}}$, has been measured as $0.003\,\mathrm{Wm}^{-2}\mathrm{Pa}^{-1}$. The evaporative coefficient at the skin surface $U^*_{\mathrm{e,cl}}$ can be related to the convective heat transfer from the surface by the Lewis number, which gives the ratio of characteristic lenghts of diffusion of mass and heat $\mathrm{Le}_{\mathrm{air}} = 0.0165\ \mathrm{KPa}^{-1}$:

$$U^*_{\mathrm{e,cl}} = \mathrm{Le}_{\mathrm{air}} h_{\mathrm{c,mix}}.$$

The spontaneous evaporative heat flux from the nude skin is equal to the driving vapour pressure difference divided by the sum of the resistances

$$\phi_e = \frac{P_{\mathrm{osk,sat}} - P_{\mathrm{v,air}}}{R_{\mathrm{e,sk}} + \frac{1}{U^*_{\mathrm{e,cl}}}}. \tag{5.5}$$

Here, $P_{\mathrm{osk,sat}}$ is the vapour pressure within the outer skin layer. Because there is always moisture present in the superficial skin layer, this is equal to the saturation vapour pressure for water at the superficial skin temperature. $P_{\mathrm{v,air}}$ is the ambient vapour pressure, it is calculated on the basis of the input ambient temperature and relative humidity.

Clothes play a key role in maintaining thermal comfort. Clothes provide a resistance against convective and radiative heat losses, as well as against evaporation. Clothing insulation, I_{cl}, is measured in Clo units, with $1\,\mathrm{clo} = 0.155\,\mathrm{m}^2\mathrm{KW}^{-1}$. A typical summer clothing ensemble has a clo value of 0.6, whereas winter clothing is about 1 clo. A full polar outfit may get up to 4 clo. The trouble when using a multi-segment thermal model is that these thermal insulation values give information on the overall effect, but don't say anything about insulation values for specific parts of the body. So, instead of using the *overall* thermal insulation values in modelling, these values are first converted into the relevant local values. Fiala did this by utilizing the numerical whole-body model itself to mimick the experiments, determining the overall parameters for a list of garments. The local effect of clothing is described with the use of three local insulation values I^*_{cl}, f^*_{cl}, and i^*_{cl}. The

effect of the air between the skin and the clothes is included in these values. The local effective heat transfer coefficient U^*_{cl} $\left[\mathrm{Wm^{-2}K^{-1}}\right]$ of multiple layers of clothing worn on a skin sector is computed as

$$U^*_{\mathrm{cl}} = \frac{1}{\sum\limits_{\mathrm{j}} (I^*_{\mathrm{cl}})_j + \frac{1}{f^*_{\mathrm{cl}}(h_{\mathrm{c,mix}}+h_{\mathrm{r}})}}.$$

The parameter $(I^*_{\mathrm{cl}})_j$ descibes the extra thermal insulation of layer j, and f^*_{cl} is the ratio of the outer surface of the clothes, from which convective and radiative transfer to the ambient will occur, to the surface of the skin. It can be seen that in principle heat transfer can also be increased due to the extra layer: this can happen if the extra layer provides little insulation but increases the surface area significantly, cf. cooling fins for electrical components.

Similarly, the evaporative coefficient $U^*_{\mathrm{e,cl}}$ including clothing now becomes

$$U^*_{\mathrm{e,cl}} = \frac{\mathrm{Le_{air}}}{\sum\limits_{\mathrm{j}} \left(\frac{I^*_{\mathrm{cl}}}{i^*_{\mathrm{cl}}}\right)_j + \frac{1}{f^*_{\mathrm{cl}} h_{\mathrm{c,mix}}}}$$

where i^*_{cl} is the local moisture permeability index of the clothing layer. The heat loss by evaporation can subsequently again be calculated according to Eq. (5.5).

Heat loss also occurs through breathing. There is both a dry heat loss because air will be warmed by the body, and there is heat loss because of evaporation in the lungs and airways. Typically respiratory heat loss accounts for more than 10% and up to 30% of the total heat loss. Since the respiratory heat losses are this significant and vary with environmental conditions and metabolic rate, it is important to model them correctly. The latent heat exchange due to evaporation of water from the lungs depends on the whole body metabolism and the difference between humidity of air breathed in and breathed out, which again depends on the ambient air temperature and the vapour pressure of the ambient air. It is modelled as, [20]

$$E_{\mathrm{rsp}} = 4.373 \times \int q_{\mathrm{m}}\, \mathrm{d}V \left(0.028 - 6.5 \times 10^{-5} T_{\mathrm{air}} - 4.91 \times 10^{-6} P_{\mathrm{v,air}}\right).$$

The air temperature T_{air} in this relation must be given as the numerical value of the temperature in degrees centigrade, the vapour pressure in Pascal. The relation is valid for a wide range of ambient conditions. The dry heat loss due to the temperature difference between inspired air and expired air can

be calculated from the air flow and the temperature and vapour pressure of the ambient air:

$$C_{\mathrm{rsp}} = 1.948 \times 10^{-3} \times \int q_{\mathrm{m}}\, \mathrm{d}V \left(32.6 - 0.066 \times T_{\mathrm{air}} - 1.96 \times 10^{-4} P_{\mathrm{v,air}}\right).$$

To account for the respiratory heat loss $E_{\mathrm{rsp}} + C_{\mathrm{rsp}}$ in the body, this loss is distributed over the body elements that model the lungs and the pulmonary tract. Most of the loss is in the nasal cavity, so most of the heat loss in the model is accounted for in the muscle layers of the face element. Only 30% of the respiratory heat loss is debited to the lungs.

5.2.3. Thermoregulation Now that most features of the model's passive system have been described, attention can be directed to the active system, which controls the passive system. The four thermoregulatory responses that need to be modelled are vasoconstriction, vasodilatation, sweating, and shivering.

The thermoregulatory responses in the model are generated by differences between actual and thermoneutral temperatures for the sensors in the body. The relevant temperatures are that of the hypothalamus, i.e. the temperature of the core node of the head, and the mean skin temperature. The thermoneutral temperatures are those temperatures that are obtained for the body if the passive model with basal values for blood flow, and metabolic rates is modelled in a thermoneutral environment. The thermoneutral state is calculated for a nude, reclining subject in an ambient temperature of 30°C, relative humidity 40%, and relative air velocity 0.05 m/s. In this situation the passive system predicts a hypothalamus temperature of 37.0°C, and a mean skin temperature of 34.4°C. Respective contributions for the heat losses in this thermoneutral state are 21.8 W for convection, 36.9 W for radiation, 19.3 W for evaporation through the skin, and 8.9 W for respiratory losses (adding up to 87 W). Basal skin flow is $0.4\,\mathrm{l\,min^{-1}}$.

The thermoregulatory relations were found by using regression analysis on measured data from a large number of experiments. It must be noted that the thermoregulatory relations described below were devised with the use of a particular passive model. The control relations work quite well, and will give a good impression of the qualitative behaviour of the thermoregulatory responses. However, these specific relations are only accurate in conjunction with the passive system with which they were developed. Significant changes in the passive system, whereas they are refinements in implementation or

different data for parameters such as skin blood flow, will require repetition of the process of developing the thermoregulatory relations that constitute the active system.

To find a control relation for shivering as a function of deviations from the thermoneutral state, about ten sets of experiments from the literature were evaluated. The heat produced by shivering was obtained by measuring the total heat output and subtracting the other contributions (basal metabolic rate and work-related). In a specific set of experiments subjects were exposed to a sudden change in environmental temperature from 24°C to 5°C. When the measured shivering was related to the temperature error signal from the skin $\Delta T_{\mathrm{sk,m}} \equiv T_{\mathrm{sk,m}} - T_{\mathrm{sk,m,0}}$, it was found that also the dynamics of the skin temperature played a role. Regression analysis on the full set of experiments involving cold exposure also showed a dependence of shivering on the core temperature.

The resulting control equation for the shiver parameter, Sh [W], in the Fiala model has the form

$$\mathrm{Sh} = 10\left[\tanh\left(0.48\Delta T_{\mathrm{sk,m}} + 3.62\right) - 1\right]\Delta T_{\mathrm{sk,m}} - 27.9\Delta T_{\mathrm{hy}} + 1.7\Delta T_{\mathrm{sk,m}}\frac{\mathrm{d}T_{\mathrm{sk,m}}}{\mathrm{d}t} - 28.6$$

In this relation, temperature differences must be entered as the numerical value of the difference in degrees centigrade. It has been found that there is a maximum to the heat that can be generated by shivering, roughly 300 to 380 W for an adult. Accordingly, shivering in the model is capped at 350 W. The place in the body where the heat is generated is in the muscle tissue of several elements. So-called shivering distribution coefficients apportion the total heat production over the elements of the body. By far the biggest portions of the shivering power are generated in the thorax (distribution coefficient 63.5%) and abdomen (24%). After the heat production for an element has been determined, this is shared out over the muscle nodes according to volume. The extra metabolic activity is accompanied by a corresponding rise in blood flow to the muscle.

Vasoaction is modelled by two control parameters that manipulate skin blood flow of an element i, SBF_i $\left[\mathrm{m^3 s^{-1}}\right]$, in the following way

$$\beta_i = \frac{\beta_{0,i} + a_{\mathrm{dl},i}\mathrm{Dl}}{1 + a_{\mathrm{cs},i}\mathrm{Cs} \times \mathrm{e}^{-\eta \mathrm{Dl}}} \times 2^{\frac{T_{\mathrm{sk},i} - T_{\mathrm{sk},i,0}}{10^{\circ}\mathrm{C}}}. \tag{5.6}$$

Here, $\beta_i = \rho_b c_b \mathrm{SBF}_i \left[\mathrm{WK}^{-1}\right]$, whereas $\beta_{0,i}$ is the corresponding basal value. Cs[−], is the vasoconstriction control parameter, and Dl is the vasodilatation control parameter $\left[\mathrm{WK}^{-1}\right]$. $a_{\mathrm{dl},i}$ and $a_{\mathrm{cs},i}$ are distribution coefficients. The Cs and Dl control parameters are whole-body parameters, so the same for all elements. Local temperatures only influence the skin blood flow through the last factor that doubles the flow for every 10°C temperature rise. This is similar but different from the other tissues where increase in blood flow is explicitly driven by the extra metabolism due to the Q_{10} effect.

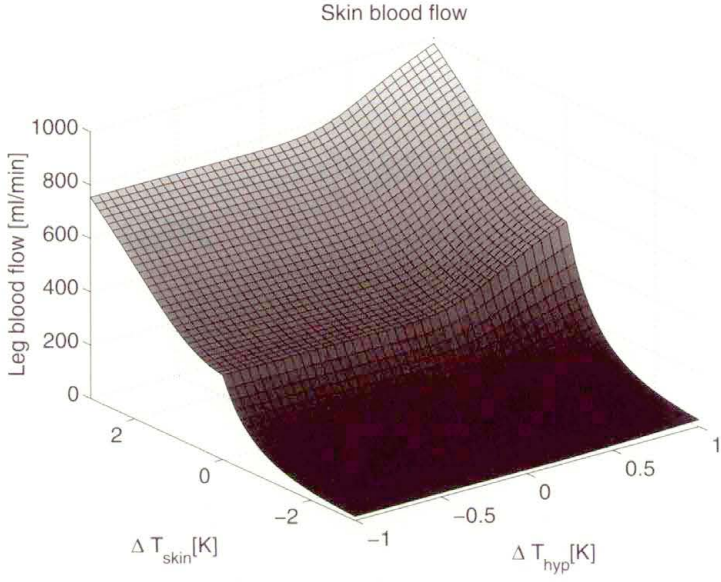

FIGURE 15. Skin blood flow in the leg as a function of difference between neutral temperatures and actual mean skin and hypothalamic temperatures. Total skin blood flow over all elements is bound by a maximum, not considered here.

The vasoconstriction parameter was a.o. derived from internal temperatures of subjects in the cold. From the regression analysis, the following control equation for the vasoconstriction parameter Cs was found

$$\mathrm{CS} = 35\left[\tanh\left(0.34\Delta T_{\mathrm{sk,m}} + 1.07\right) - 1\right]\Delta T_{\mathrm{sk,m}} + 3.9\Delta T_{\mathrm{sk,m}}\frac{\mathrm{d}T_{\mathrm{sk,m}}}{\mathrm{d}t} \quad (5.7)$$

Thus, also the vasoconstriction is dependent on dynamic skin temperature behaviour, but it is not directly dependent on the hypothalamus temperature. The relation is only valid for low temperatures: if the vasoconstriction parameter falls below zero, the value zero is used in Eq. (5.6). Likewise, the

dynamic term in Eq. (5.7) is only pertinent for dropping skin temperatures and is omitted for rising temperatures.

The regression analysis for the vasodilatation parameter Dl involved experiments in hot environment and/or exercise. The analysis resulted in

$$\mathrm{Dl} = 21\,[\tanh(0.79\Delta T_{\mathrm{sk,m}} - 0.70) + 1]\,\Delta T_{\mathrm{sk,m}} + 32\,[\tanh(3.29\Delta T_{\mathrm{hy}} - 1.46) + 1]\,\Delta T_{\mathrm{hy}}.$$

Again, only if the relation results in a positive value for Dl is the outcome used in Eq. (5.6), otherwise zero is used. Also, there is a maximum to the total skin blood flow. This maximum is dependent on how much of the cardiac output is required by the muscles.

The heat loss from sweating was obtained from experiments by taking the overall measured latent loss and subtracting respiratory losses and the predicted amount of spontaneous moisture diffusion through the skin $E_{\mathrm{sw}} = E_{\mathrm{exp}} - (E_{\mathrm{rsp}} + E_{\mathrm{diff}})$ [W]. In the regression analysis, the sweat control variable $\mathrm{Sw}\left[\mathrm{g\,min^{-1}}\right]$ was derived from the heat loss through

$$\mathrm{Sw} = \frac{E_{\mathrm{sw}} \times 6 \times 10^4}{\lambda_{\mathrm{H_2O}} \sum_{\mathrm{i}} a_{\mathrm{sw},i} \times 2^{\frac{T_{\mathrm{sk},i} - T_{\mathrm{sk},i,0}}{10^{\circ}\mathrm{C}}}}.$$

The number in the numerator is for the unit conversion from kg/s to the more convenient g/min. The $\lambda_{\mathrm{H_2O}} = 2256\,\mathrm{kJ\,kg^{-1}}$ is the heat of vaporization of water. The last factor in the denominator takes into account how eventually the local sweat rates are calculated from the sweat parameter. That is, local sweat rates are dependent on the local skin temperature

$$\mathrm{Sw}_i = a_{\mathrm{sw},i} \times \mathrm{Sw} \times 2^{\frac{T_{\mathrm{sk},i} - T_{\mathrm{sk},i,0}}{10^{\circ}\mathrm{C}}}.$$

In a hot environment a rise in skin temperature will trigger sweating, whereas an increase in core temperature is the main driving influence during exercise in cool conditions. The regression analysis resulted in

$$\mathrm{Sw} = [0.8\tanh(0.59\Delta T_{\mathrm{sk,m}} - 0.19) + 1.2]\,\Delta T_{\mathrm{sk,m}} + [5.7\tanh(1.98\Delta T_{\mathrm{hy}} - 1.03) + 6.3]\,\Delta T_{\mathrm{hy}}.$$

This relation takes into account that a lower than normal hypothalamic temperature counteracts the effect on sweating of higher than normal skin temperatures, and vice versa. The maximum rate of sweating for an adult is

approximately $30\,\mathrm{g\,min^{-1}}$, and this is the value at which sweating is capped in the model. The resulting evaporation heat loss including sweating can be found by adding the extra vapour flow to the spontaneous diffusion in the skin:

$$\phi_{e,i} = U^*_{e,cl}\,(P_{sk,i} - P_{v,air}) = \frac{\lambda_{H_2O}}{A_{sk,i}}\mathrm{Sw}_i + \frac{P_{osk,i,sat} - P_{sk,i}}{R_{e,sk}} \tag{5.8}$$

Because the vapour pressure at the skin surface $P_{sk,i}$ can be evaluated by re-arranging Eq. (5.8), the evaporative heat loss can be calculated. A further complication is that sweat is accumulated if the skin surface vapour pressure is higher than the saturation vapour pressure. The model does account for storage of sweat in that case.

6. Discussion of the Whole-body Thermal Models

For the many graphs of the regression analysis and examples of the behaviour of the resulting model under different conditions the reader is referred to the original papers, [16, 17]. By and large the model does well in predicting the average thermal behaviour of groups subjected to a variety of thermal conditions. This is to be expected as over the test group, both the anatomy and also the less tangible stable and transient individual characteristics will tend to the average. It is of course a prerequisite that the base underlying model system gives a reasonable description of the real system, and the themoregulatory relations are based on a large amount of data. However, even the average experimental results for groups are sometimes significantly different from model predictions. This can in part be attributed to the usually small group size for this type of experiments, but also to systematic differences between what may seem similar experiments. Typically, to reduce confounding factors, an experiment on a group will be standardized with respect to initial conditions, but this can lead to some systematic differences between experiments. Cultural, climatic, and population differences between studies may also play a role.

Not every single feature of the numerical model by Fiala has been included in the above description. Nonetheless, the account should have given the interested reader a feeling for the complexities involved. It should not come as a surprise that the model will not as a simple matter predict highly accurate absolute temperature distributions for an arbitrary individual under every succession of conditions. To get good individual predictions from the model,

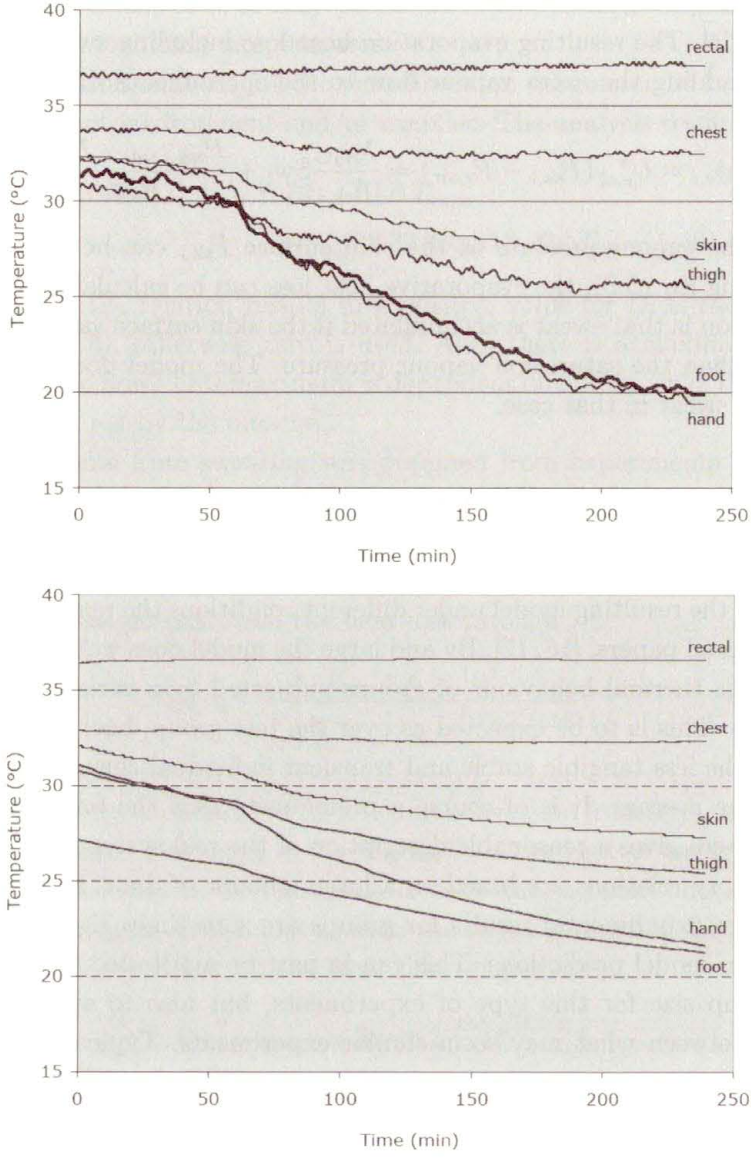

Figure 16. Measured (top) and modelled (bottom) temperatures for cold exposure, Fiala model adapted for the individual subject, [21].

the model should be tailored to the individual, Fig. 16. Adapting the model anatomy of the standard human to reflect the true height, weight and fat percentage of the individual may be easily done. Other individual properties, such as the basal metabolic rate, may be less readily measured, as well as they

might be less constant in time. It will be difficult to very precisely predict the temperature distribution for an individual in irregular conditions. If there is a clinical interest in predicting these temperatures, data should be collected for these specific conditions and the model correspondingly updated. This may eventually lead to an even more dynamic model. For the individual patient, the accuracy of predictions can be further increased by updating characteristics of the model real-time on the basis of measurements during the procedure.

References

1. H.H. PENNES, *Analysis of tissue and arterial blood temperature in the resting human forearm*, Journal of Applied Physiology, **1**: 93–122, 1948
2. W. WULFF, *The energy conservation equation for living tissue*, IEEE Transactions on Biomedical Engineering, **21**: 494–495, 1974
3. M.M. CHEN and K.R. HOLMES, *Microvascular contributions in tissue heat transfer*, Annals of the New York Academy of Sciences, **335**: 137–151, 1980
4. S. WEINBAUM and L.M. JIJI, *A new simplified bioheat equation for the effect of local average tissue temperature*, ASME Journal of Biomechanical Engineering, **107**: 131–139, 1985
5. J.W. BAISH, P.S. AYYASWAMY, and K.R. FOSTER, *Heat transport mechanisms in vascular tissues: A model comparison*, ASME Journal of Biomechanical Engineering, **108**: 324–331, 1986
6. W.M. KAYS and M.E. CRAWFORD, *Convective heat and mass transfer*, McGraw-Hill Book Company, New York 1980
7. J. CREZEE, J. MOOIBROEK, C.K. BOS, and J.J.W. LAGENDIJK, *Interstitial heating: experiments in artificially perfused tongues*, Physics in Medicine and Biology, **36**: 823–833, 1991
8. R.J. RAWNSLEY, R.B. ROEMER, and A.W. DUTTON, *The simulation of discrete vessel effects in experimental hyperthermia*, Journal of Biomechanical Engineering, **116**: 256–262, 1994
9. J.F. VAN DER KOIJK, J. CREZEE, G.M.J. VAN LEEUWEN, J.J. BATTERMANN, and J.J.W. LAGENDIJK, *Dose uniformity in MECS interstitial hyperthermia: the impact of longitudinal control in model anatomies*, Physics in Medicine and Biology, **41**: 429–444, 1996
10. J. CREZEE and J.J.W. LAGENDIJK, *Temperature uniformity during hyperthermia: the impact of large vessels*, Physics in Medicine and Biology, **37**: 1321–1337, 1992
11. A.N.T.J. KOTTE, G.M.J. VAN LEEUWEN, J. DE BREE, J.K. VAN DER KOIJK, and J.J.W. LAGENDIJK, *A description of discrete vessel segments in thermal modelling of tissues*, Physics in Medicine and Biology, **41**: 865–884, 1996

12. G.M.J. Van Leeuwen, A.N.T.J. Kotte, J. Crezee, and J.J.W. Lagendijk, *Tests of the geometrical description of blood vessels in a thermal model using countercurrent geometries*, Physics in Medicine and Biology, **42**: 1515–1532, 1997

13. G.M.J. Van Leeuwen, *Numerical modelling of heat transfer in hyperthermia*, PhD Thesis, Universiteit Utrecht, 1998

14. G.M.J. Van Leeuwen, J.J.W. Lagendijk, B.J.A.M. Van Leersum, A.P.M. Zwamborn, S.N. Hornsleth, and A.N.T.J. Kotte, *Calculation of change in brain temperatures due to exposure to a mobile phone*, Physics in Medicine and Biology, **44**:2367–2379, 1999

15. A.P. Gagge, J.A.J. Stolwijk, and Y. Nishi, *An effective temperature scale based on a simple model of human physiological regulatory response*, ASHRAE Trans, **77**: 247–257, 1971

16. D. Fiala, K.J. Lomas, and M. Stohrer, *A computer model of human thermoregulation for a wide range of environmental conditions: The passive system*, Journal of Applied Physiology, **87**: 1957–1972, 1999

17. D. Fiala, K.J. Lomas, and M Stohrer, *Computer prediction of human thermoregulatory and temperature responses to a wide range of environmental conditions*, International Journal of Biometeorology, **45**: 143–159, 2001

18. P. Höppe, *The physiological equivalent temperature—a universal index for the biometeorological assessment of the thermal environment*, International Journal of Biometeorology, **43**: 71–75, 1999

19. J.A.J. Stolwijk, *A mathematical model of physiological temperature regulation in man*, NASA contractor report CR-1855, Washington DC, 1971

20. P.O. Fanger, Thermal Comfort—Analysis and Applications in Environmental Engineering, McGraw-Hill Book Company, New York 1973

21. W.D. van Marken Lichtenbelt, A.J.H Frijns, A.M.J. van Ooijen, D.Fiala, A. Kester, and A.A. van Steenhoven, *Validation of an individualized model of human thermoregulation for predicting responses to cold*, submitted